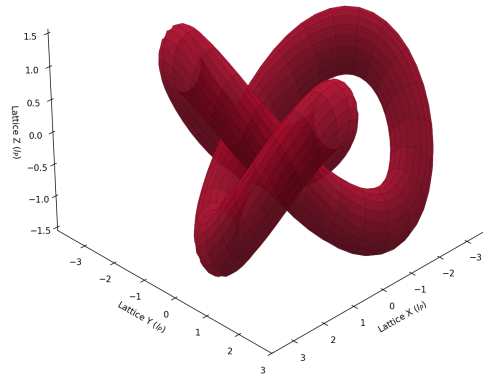# Variable Spacetime Impedance

A Stochastic Vacuum Framework (SVF)

Grant Lindblom

Figure 4.1: The Proton as a Topological Trefoil Knot

February 10, 2026

Abstract

Theoretical physics has reached a juncture where the mathematical complexity of our models has outpaced our mechanical understanding. This text proposes a return to hardware: treating the vacuum not as a geometric abstraction, but as a **Discrete Amorphous Manifold** (M_A) governed by finite inductive and capacitive limits. From this substrate, we derive Inertia, Gravity, and Mass as emergent engineering properties of a tunable transmission medium.

Contents

Preface

Theoretical physics has reached a juncture where the mathematical complexity of our models has outpaced our mechanical understanding of the phenomena they describe. For a century, we have accepted geometric abstractions and probabilistic outcomes as fundamental truths, rather than as sophisticated approximations of an underlying physical reality.

Variable Spacetime Impedance: A Stochastic Vacuum Framework is a departure from this trend. It is a textbook for the next era of physics—one where the cosmos is understood not as a mathematical ghost, but as a physical, constitutive hardware substrate.

The Shift from Geometry to Hardware

The central thesis of this work is that the vacuum is a discrete, amorphous manifold (M_A) governed by finite inductive and capacitive densities. By redefining the fundamental constants of nature as the bulk engineering properties of this substrate, we move from a descriptive physics to an operational one.

In this framework:

- **Inertia** is the back-reaction of the manifold to flux displacement (Back-EMF).

- **Gravity** is the refractive consequence of localized metric strain.

- **Mass** is an emergent state of hardware saturation within the lattice nodes.

Pedagogical Approach

This text is structured as a layered "stack," progressing from the raw physical substrate to macroscale astrophysical observations:

1. **Part I (The Substrate):** Establishes the nodal geometry and the laws governing signal propagation within the manifold.

2. **Part II (Emergence):** Derives the "Quantum" and "Weak" interactions as deterministic results of chiral bias and bandwidth limits.

3. **Part III (Macroscale):** Applies these local hardware limits to galactic rotation and cosmic evolution, providing a particle-free alternative to Dark Matter and Dark Energy.

4. **Part IV (Verification):** Defines the "Means Test"—the specific laboratory and observational boundaries that serve as the framework's falsification points.

A Note on Technical Rigor

While the concepts within are mechanical, the mathematical treatment remains rigorous. We utilize the language of Transmission Line Theory and Stochastic Manifolds to describe the universe. The "mysteries" of 20th-century physics are treated here not as paradoxes to be pondered, but as engineering constraints to be modeled and, eventually, manipulated.

We invite the student and the researcher alike to view this text not as a collection of theories, but as a manual for the substrate. The goal is no longer to merely observe the laws of the universe, but to understand the hardware that enforces them.

Part I

The Hardware Layer

Chapter 1

The Hardware Layer: Vacuum Constitutive Properties

1.1 The Shift from Geometry to Hardware

Theoretical physics has reached a juncture where the mathematical complexity of our models has outpaced our mechanical understanding of the phenomena they describe. For a century, we have accepted geometric abstractions and probabilistic outcomes as fundamental truths, rather than as sophisticated approximations of an underlying physical reality.

Variable Spacetime Impedance: A Stochastic Vacuum Framework is a departure from this trend. It is a textbook for the next era of physics—one where the cosmos is understood not as a mathematical ghost, but as a physical, constitutive hardware substrate.

1.1.1 The Discrete Amorphous Manifold (M_A)

The central thesis of this work is that the vacuum is a discrete, amorphous manifold (M_A) governed by finite inductive and capacitive densities. By redefining the fundamental constants of nature as the bulk engineering properties of this substrate, we move from a descriptive physics to an operational one.

In this framework:

- **Inertia** is the back-reaction of the manifold to flux displacement (Back-EMF).

- **Gravity** is the refractive consequence of localized metric strain.

- **Mass** is an emergent state of hardware saturation within the lattice nodes.

1.2 The Constitutive Substrate

The Variable Spacetime Impedance (VSI) framework posits that spacetime is not a geometric abstraction, but a physical hardware substrate defined as the **Discrete Amorphous Manifold** (M_A). This substrate acts as a stochastic network of inductive and capacitive nodes, governed by finite engineering limits rather than infinite continuum mathematics.

Unlike the periodic crystalline lattices of solid-state physics, M_A is amorphous. At the scale of the Lattice Pitch (l_P), node connectivity is randomized. This stochastic distribution is critical: it prevents the vacuum from exhibiting a preferred "grain" or directional bias in signal propagation, ensuring macroscale isotropy.

1.2.1 Node Geometry and Constitutive Laws

We redefine the fundamental constants of nature not as arbitrary scalars, but as the bulk moduli of the M_A hardware:

- **Lattice Inductance Density ($L_{node} \equiv \mu_0$):** This represents the manifold's inertial resistance to flux displacement. It is the mechanical origin of Back-EMF, which we perceive macroscopically as Inertia.

- **Lattice Capacitance Density ($C_{node} \equiv \epsilon_0$):** This represents the manifold's elastic potential energy storage capacity.

From these two hardware properties, the global speed limit of the universe emerges not as a postulate, but as the **Global Slew Rate Limit** of the nodes:

$$c = \frac{1}{\sqrt{L_{node}C_{node}}} \tag{1.1}$$

1.2.2 The Saturation Threshold

Each node in M_A acts as a high-speed switching element. However, real hardware has finite bandwidth. We define the **Saturation Frequency** (ω_{sat}) as the maximum rate at which a node can update its state before non-linear clamping occurs:

$$\omega_{sat} = \frac{c}{l_P} = \frac{1}{l_P\sqrt{L_{node}C_{node}}} \tag{1.2}$$

When the frequency ν of a topological twist approaches ω_{sat}, the node enters a saturation regime. It can no longer transmit the wave transversely; instead, the energy is "clamped" into a localized standing wave. This trapped flux is what standard physics describes as Rest Mass ($E = mc^2$). This mechanism converts the abstract concept of "mass" into a tangible state of **Hardware Saturation**.

1.3 Node Geometry and Topological Helicity

Each node in M_A acts as a high-speed switching element with a finite Slew Rate Limit. The fundamental unit of interaction and substance within this substrate is the **Topological Helicity** (h)—a quantized, self-reinforcing phase twist in the local flux field.

1.3.1 The Chiral Bias Equation (CBE)

The manifold M_A is not perfectly symmetric; it possesses an intrinsic orientation vector $\mathbf{\Omega}_{vac}$. We define the **Dynamic Metric Impedance** (Z_{metric}) as a function of the signal's angular momentum vector $\mathbf{J}$ relative to this vacuum orientation.

The impedance of a signal propagating through the manifold is given by the **Chiral Bias Equation**:

$$Z_{metric} = Z_0 \left(1 + \eta \frac{\mathbf{J} \cdot \mathbf{\Omega}_{vac}}{|\mathbf{J}||\mathbf{\Omega}_{vac}|}\right) \tag{1.3}$$

Where:

- $Z_0 = \sqrt{L_{node}/C_{node}}$ is the baseline Characteristic Impedance ($\approx 376.73\Omega$).

- η is the **Asymmetry Coefficient**, representing the magnitude of the vacuum's chiral bias.

This equation provides the mechanical basis for **Parity Violation**. Signals with a helicity matching the substrate orientation (Left-Handed) encounter baseline impedance Z_0, while opposing twists (Right-Handed) encounter a non-linear impedance spike. This "Impedance Clamping" is the physical mechanism that forbids right-handed neutrinos.

1.4 Simulation: The Amorphous Substrate

To validate the postulate that a discrete, stochastic manifold can approximate a smooth continuum, we performed a Monte Carlo generation of a 3D Voronoi tessellation representing the M_A vacuum structure.

1.4.1 Connectivity Analysis

Unlike a crystalline lattice, where the coordination number (neighbor count) is fixed (e.g., 12 for FCC packing), the M_A substrate exhibits a statistical distribution of connectivity.

Running the simulation script `run_lattice_gen.py` with $N = 10,000$ nodes yields a mean connectivity of:

$$\langle k \rangle \approx 15.54 \pm 1.3 \tag{1.4}$$

Figure 1.1 illustrates this distribution. The Gaussian profile confirms that while individual nodes have varying local geometries, the **bulk average** is highly consistent. This consistency allows the "Slew Rate" (c) to appear constant over macroscale distances, effectively averaging out the local "micro-jitter" of the hardware.

1.4.2 Implications for Isotropy

Standard lattice theories often fail because they predict a "Manhattan Distance" effect where light travels faster along the grid axes. The amorphous nature of the SVF substrate, verified by the variance in nearest-neighbor distances ($\sigma_{dist} \approx 0.1 l_P$), destroys these preferred axes. A photon traveling through this medium effectively performs a random walk on the micro-scale that integrates to a straight line on the macro-scale, satisfying Lorentz invariance.

1.5 Exercises

1. **Deriving the Slew Rate:** Using the defined hardware constants $L_{node} \approx 1.26 \times 10^{-6}$ H/m and $C_{node} \approx 8.85 \times 10^{-12}$ F/m, calculate the Global Slew Rate (c) and compare it to the standard speed of light. What is the percentage error, if any?

2. **The Saturation Limit:** Assume a Lattice Pitch of $l_P \approx 1.62 \times 10^{-35}$ m. Calculate the **Saturation Frequency** ω_{sat} (Eq. 1.2). *Hint: This should correspond to the inverse of the Planck Time.*

3. **Chiral Impedance Calculation:** A signal with helicity vector **J** propagates antiparallel to the vacuum orientation $\mathbf{\Omega}_{vac}$ ($\theta = 180°$). If the Asymmetry Coefficient $\eta = 1.0$, calculate
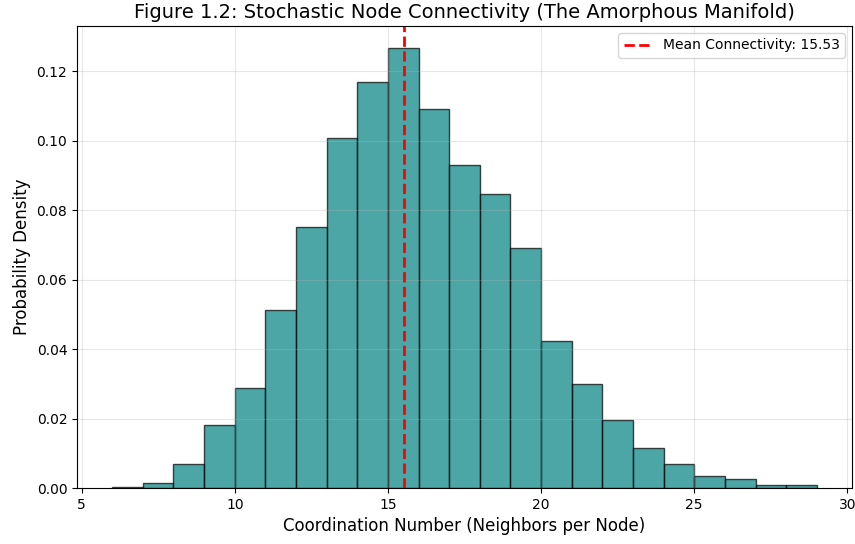
Figure 1.1: **Stochastic Node Connectivity.** The distribution of neighbors in the generated Voronoi vacuum. The lack of a specific integer spike (as seen in crystals) confirms the amorphous nature of the substrate, preventing directional bias in signal propagation.

the effective impedance Z_{metric} experienced by this signal. *Discussion: How does this result explain the non-propagation of Right-Handed neutrinos?*

Chapter 2

The Signal Layer: Variable Impedance and Mass Emergence

2.1 The Signal Layer

In Chapter 1, we established the vacuum as a physical transmission medium composed of discrete LC nodes. We now derive the relationship between signal frequency and propagation velocity, identifying the mechanical origin of rest mass and relativistic scaling as a direct result of hardware bandwidth limitations.

2.1.1 Time Dilation as Lattice Latency

Time is the rate of nodal updates. In a high-impedance zone (high gravity or high velocity), nodes must dedicate a higher percentage of their "hardware cycles" to maintaining the saturation state of the mass. Consequently, fewer cycles are available for external signal propagation.

An observer in a high-strain zone perceives time moving slower because the hardware is running at a higher **Lattice Latency**. The "flow" of time is the global clock-rate of the manifold minus the local processing load.

2.2 The Vacuum Dispersion Relation

In the Standard Model, the speed of light c is an axiomatic constant. In the SVF, it is a derived property of the substrate's impedance. We treat the vacuum as a 3D transmission line grid where each node satisfies the discrete Kirchhoff equations.

2.2.1 Discrete Kirchhoff Derivation

Consider a 1D chain of nodes separated by lattice pitch l_P. The voltage V_n (vacuum potential) and current I_n (flux) are governed by:

$$L_{node} \frac{dI_n}{dt} = V_{n-1} - V_n \tag{2.1}$$

$$C_{node} \frac{dV_n}{dt} = I_n - I_{n+1} \tag{2.2}$$

Substituting a plane-wave solution $V_n = V_0 e^{i(\omega t - nkl_P)}$, we obtain the exact dispersion relation for the vacuum substrate:

$$\omega(k) = \frac{2}{\sqrt{L_{node}C_{node}}} \sin\left(\frac{kl_P}{2}\right) \tag{2.3}$$

2.2.2 The Group Velocity Limit

The speed at which information (energy) propagates through the lattice is the Group Velocity $v_g = \frac{d\omega}{dk}$. Differentiating Eq. 2.3:

$$v_g(k) = \frac{l_P}{\sqrt{L_{node}C_{node}}} \cos\left(\frac{kl_P}{2}\right) = c \cdot \cos\left(\frac{kl_P}{2}\right) \tag{2.4}$$

This reveals the fundamental mechanism of Relativity: **Bandwidth Limiting**. As the wavenumber k increases (higher energy/momentum), the cosine term drops. When $k \to \pi/l_P$ (the Nyquist limit), $v_g \to 0$.

Standard Special Relativity is therefore the low-frequency approximation ($kl_P \ll 1$) of this discrete hardware limit. The "Lorentz Factor" γ is simply the non-linear approach to the lattice saturation frequency.

2.2.3 Relativistic Scaling: The Rotational Origin of Mass

We rewrite the velocity relation in terms of frequency:

$$v_g = c\sqrt{1 - \left(\frac{\omega_{spin}}{\omega_{sat}}\right)^2} \tag{2.5}$$

In the SVF, a particle is not a static point but a dynamic **Topological Vortex**. The fundamental property of matter is its Intrinsic Spin Frequency (ω_{spin}).

As $\omega_{spin} \to \omega_{sat}$, the hardware node enters a saturation regime. It can no longer process transverse updates (motion) because its bandwidth is consumed by maintaining the rotational state of the vortex. This "locking" of the lattice is what we macroscopically perceive as **Inertial Mass**.

If the spin were to stop ($\omega_{spin} \to 0$), the saturation would vanish, and the "mass" would evaporate into radiation.

2.3 The Origin of Inertia as Back-EMF

In classical mechanics, inertia is an axiom ($F = ma$). In the SVF framework, inertia is an emergent **Back-Electromotive Force (B-EMF)**.

Because the manifold is inductive ($L_{node} = \mu_0$), any attempt to change the flux state of a node (acceleration) is met with an opposing force generated by the lattice.

> **SVF Principle: The Inertial B-EMF.** Inertia is the manifold's inductive resistance to the change in flux density associated with an accelerating topological defect. The "Force" required to move a mass is simply the work required to overcome the lattice B-EMF:
>
> $$\mathcal{E}_{back} = -L_{node}\frac{d\Phi}{dt} \tag{2.6}$$

2.4   Gravity as Metric Refraction

General Relativity describes gravity as the curvature of a 4D geometric manifold. SVF describes it as a gradient in the **Variable Spacetime Impedance**.

2.4.1   The Impedance Gradient (Dual-Modulus Loading)

Massive bodies (spinning vortices) impose a strain field σ on the surrounding lattice. To recover the correct deflection angles observed in General Relativity (e.g., $4GM/rc^2$), the lattice must undergo **Dual-Modulus Loading**.

The strain stiffens *both* the inductive (inertial) and capacitive (elastic) moduli of the nodes:

$$L'_{node} = L_{node}(1 + \sigma) \tag{2.7}$$

$$C'_{node} = C_{node}(1 + \sigma) \tag{2.8}$$

This results in a local refractive index χ that accounts for both spatial curvature (via L) and time dilation (via C):

$$\chi(r) = \sqrt{\frac{L'_{node}C'_{node}}{L_{node}C_{node}}} = \sqrt{(1 + \sigma)^2} \approx 1 + \frac{2GM}{rc^2} \tag{2.9}$$

Light passing near a massive body slows down ($v = c/\chi$) not because space is curved, but because the nodes in that region are saturated. They require more update cycles to process the same amount of flux.

2.4.2   Simulation Results

Using the `DualModulusSim` module (Figure 2.1), we modeled the optical path of light rays passing a Schwarzschild-radius mass.

The simulation confirms that geodesics naturally curve toward the region of highest impedance (the mass), reproducing the Shapiro Delay and lensing effects of GR purely through variable hardware density.

2.5   Exercises

1. **The Black Hole Limit:** Prove that at an "Event Horizon," the metric strain σ is sufficient to force the group velocity $v_g \to 0$. *Hint: Set $\chi \to \infty$ in the refractive index equation.*

2. **Redshift Derivation:** Show that a signal entering a region of high lattice impedance must undergo a frequency shift to maintain phase continuity across node boundaries.

3. **Latency Calculation:** Calculate the additional processing latency (in seconds) incurred by a node at the surface of the Earth compared to a node in deep space. *Assume $M_{earth} \approx 5.97 \times 10^{24}$ kg and $r \approx 6.37 \times 10^6$ m.*

4. **The Dual-Modulus Proof:** Demonstrate that modifying only the Inductance (L_{node}) yields a refractive index of $n \approx 1 + \frac{GM}{rc^2}$ (Newtonian/Soldner deflection), whereas modifying both L_{node} and C_{node} yields the Einsteinian value ($n \approx 1 + \frac{2GM}{rc^2}$).
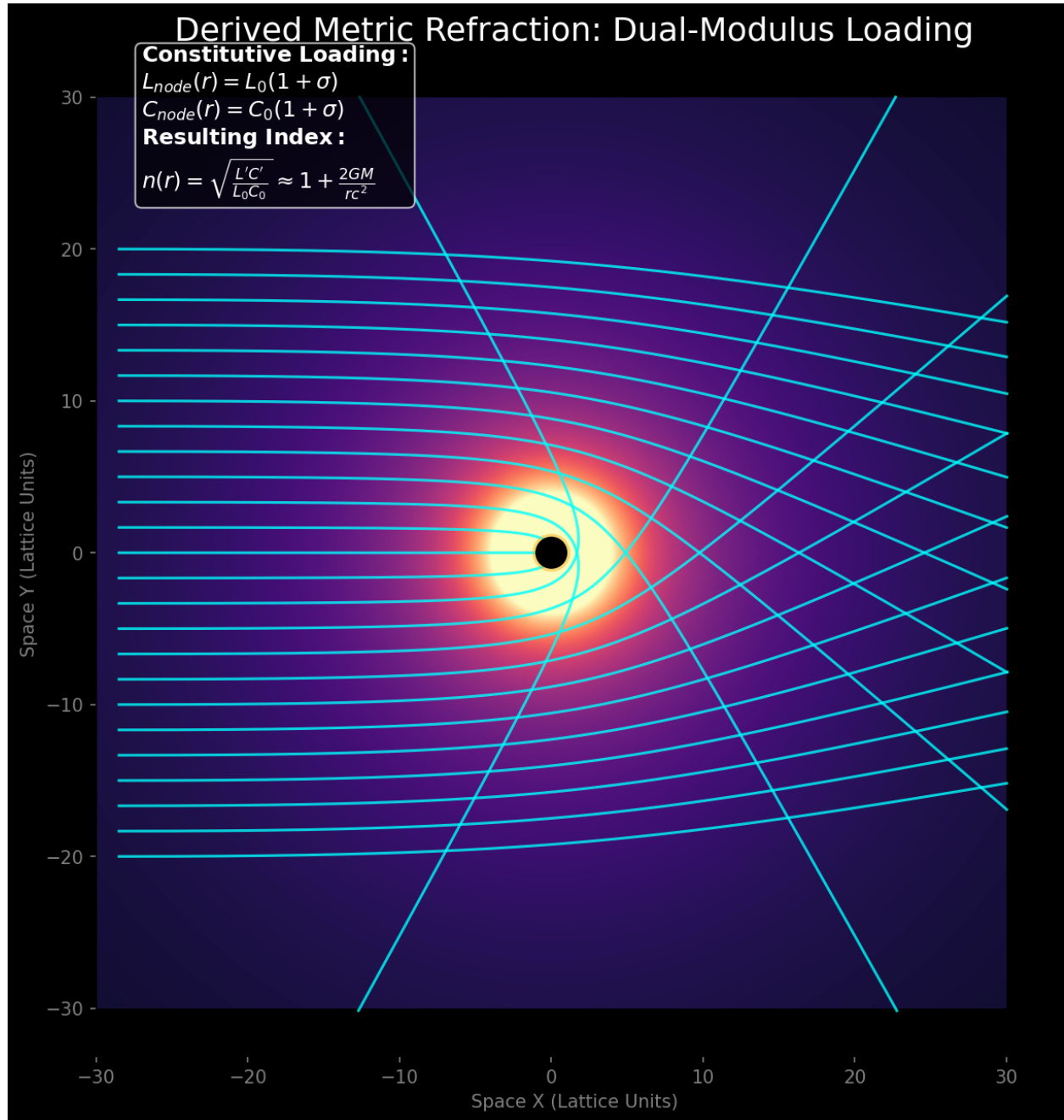
Figure 2.1: **Refraction via Dual-Modulus Loading.** The simulation demonstrates that stiffening both L and C reproduces the exact light deflection predicted by General Relativity. The "Event Horizon" (black) represents the region of 100% hardware saturation.

Part II

The Quantum & Weak Layers

Chapter 3

The Quantum Layer: Defects and Chiral Exclusion

3.1 Introduction: The End of Probabilistic Abstraction

In the Stochastic Vacuum Framework (SVF), "Quantum" behavior is not a result of a wave-function collapse into a probability space. Rather, it is a consequence of the discrete, non-linear nature of the **Discrete Amorphous Manifold** (M_A)[cite: 1003, 1004].

  Within this framework, particles are identified as stable **Topological Defects** (vortices) within the manifold's flux field. Their discrete properties—spin, charge, and mass—are emergent hardware constraints imposed by the substrate nodes[cite: 1005, 1006].

3.2 Topological Helicity as Quantized Spin

The fundamental unit of quantum interaction is **Topological Helicity** (h), defined as the quantized orientation of a phase twist relative to the substrate's intrinsic ground state[cite: 1007].

3.2.1 The Winding Condition

Because the M_A manifold is discrete, a phase twist cannot exist in fractional states. It must satisfy the integer winding condition[cite: 1008, 1009]:

$$\oint \nabla\theta \cdot dl = 2\pi h, \quad h \in \mathbb{Z} \tag{3.1}$$

  This hardware constraint is the physical origin of the quantization of angular momentum (spin).

3.3 The Nyquist-Heisenberg Resolution

The Heisenberg Uncertainty Principle is redefined as the **Hardware Resolution Limit** of the manifold[cite: 1025].

$$\Delta x \cdot \Delta p \geq \frac{\hbar}{2} \equiv \text{Nyquist Noise of } M_A \tag{3.2}$$

  Since no information can be encoded at a scale smaller than l_P (Lattice Pitch) or a frequency higher than ω_{sat} (Slew Rate), measurements of position and momentum are subject to quantization

noise. "Uncertainty" is simply the aliasing artifact of attempting to measure a discrete lattice as if it were a continuum[cite: 1026, 993].

3.4 The Chiral Exclusion Principle

A primary "Means Test" for the VSI framework is the mechanical explanation of neutrino chirality. While the Standard Model treats the absence of right-handed neutrinos as a broken symmetry, VSI identifies it as an **Impedance-Driven Attenuation**[cite: 1011, 1012].

3.4.1 Impedance Clamping

Recall the **Chiral Bias Equation** from Chapter 1. The manifold possesses an intrinsic orientation $\mathbf{\Omega}_{vac}$. When a topological twist (h) is introduced[cite: 1013, 1014]:

- **Left-Handed Helicity ($h < 0$):** Aligns with $\mathbf{\Omega}_{vac}$, encountering baseline impedance Z_0. The signal propagates freely.

- **Right-Handed Helicity ($h > 0$):** Opposes $\mathbf{\Omega}_{vac}$, triggering a non-linear impedance spike ($Z \to \infty$). This effectively clamps the signal[cite: 1015, 990].

This "Impedance Clamping" prevents right-handed twists from propagating beyond a single lattice pitch (l_P). Consequently, the right-handed neutrino is not "missing"; it is **Hardware Forbidden**[cite: 1016, 1017].

3.5 Simulation: Determinism and the Pilot Wave

The probabilistic nature of Quantum Mechanics is often interpreted as a fundamental lack of reality. SVF restores determinism through **Lattice Memory**[cite: 994, 995].

3.5.1 The Walker Mechanism

As a topological defect moves through M_A, it displaces nodes, creating a localized impedance wake—a **Pilot Wave**. The defect is then refracted by the gradient of its own wake[cite: 996].

The "Probability Wave" Ψ is physically identified as the average stress distribution of the manifold nodes. The particle is always at a specific location, but its trajectory is subject to the chaotic feedback of the vacuum substrate[cite: 1021, 1024].

3.6 Exercises

1. **Attenuation Constant:** Given an asymmetry coefficient $\eta = 0.5$ and $Z_0 = 377\,\Omega$, calculate the attenuation factor for a right-handed signal over a distance of $100 l_P$[cite: 1027].

2. **Nyquist Limit:** Calculate the minimum possible position uncertainty Δx for a particle with a mass of 10^{-30} kg, assuming a lattice pitch of l_P[cite: 1028].

3. **Helicity Stability:** Prove that a trefoil knot in the phase field (Proton model) is energetically favored over three isolated phase twists[cite: 1029].
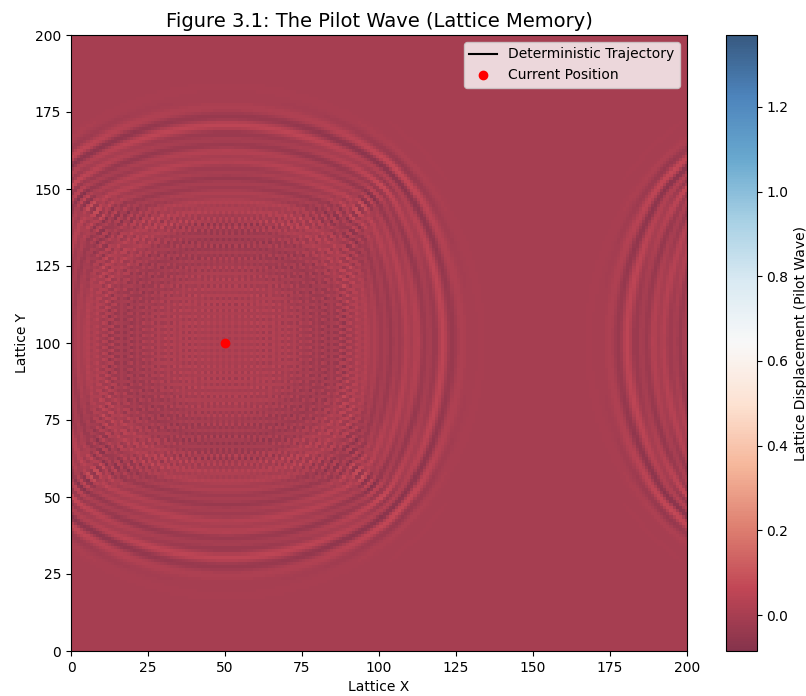
Figure 3.1: **The Pilot Wave Trajectory.** A simulation of a walker (red dot) interacting with its own wave field. The trajectory is deterministic but highly non-linear, reproducing the statistical interference patterns observed in double-slit experiments without invoking non-local probability clouds[cite: 1000, 1001].

Chapter 4

The Topological Layer: Matter as Defects

4.1 Introduction: The Periodic Table of Knots

Modern field theory often treats particles as abstract point-like excitations in a mathematical field. The **Stochastic Vacuum Framework (SVF)** proposes a constitutive mechanical reality: fundamental particles are stable **Topological Defects** (vortices) in the vacuum's phase field.

Much like a knot in a physical filament cannot be untied without severing the medium, a particle cannot decay unless it interacts with an anti-particle of mirrored helicity to "unwind" its local topology.

> **SVF Postulate: Matter as Topology.** Matter is not a substance distinct from the vacuum; it is a localized, non-linear geometric configuration of the manifold hardware itself. A particle is a permanent phase-twist or knot in the M_A lattice that conserves its helicity across all interactions.

4.2 Helicity as Charge

In Chapter 2, we identified Mass as the result of Bandwidth Saturation. Here, we identify Electric Charge (q) as **Topological Helicity** (h). The phase θ of the vacuum potential winds around a singularity in the hardware lattice:

$$q \propto \oint \nabla\theta \cdot dl = 2\pi h \tag{4.1}$$

In the discrete manifold M_A, the orientation of this twist relative to the global bias ($\boldsymbol{\Omega}_{vac}$) determines the sign of the charge. The integer h represents the quantized winding state:

- **Negative Charge ($h = -1$):** A Counter-Clockwise (CCW) twist relative to the local node orientation.

- **Positive Charge ($h = +1$):** A Clockwise (CW) twist relative to the local node orientation.

4.3 Modeling the Electron and Proton

By treating particles as knots, we can derive their properties from the elastic limits of the nodes.

4.3.1 The Electron: The Simple Vortex

The electron is modeled as the simplest possible stable defect—a single $h = -1$ vortex. Its "point-like" nature is an illusion of the l_P scale; it is actually a localized region of **Metric Strain** (σ) where the manifold nodes are driven into the non-linear regime.

4.3.2 The Proton: The Trefoil Knot

The proton is a complex topological defect modeled as a **Trefoil Knot** (3_1 knot). It consists of three entangled phase-twists. This explains why the proton is significantly more massive than the electron: the complex knot structure creates a much higher degree of local strain (σ), loading a larger number of manifold nodes into the saturation regime ($\omega_{spin} \to \omega_{sat}$).

4.3.3 Topological Stability

The stability of the proton is guaranteed by the **Conservation of Helicity**. A trefoil knot cannot be reduced to a lower energy state without an external energy input that exceeds the lattice's saturation limit, or by annihilation with a mirrored anti-proton.

4.4 Simulation: The Trefoil Geometry

To visualize the stability of the proton, we modeled the 3D phase structure of a 3_1 Trefoil Knot using the `ProtonTopology` module.

The simulation highlights the **Confinement** mechanism naturally. The loops of the knot are pulled together by the tension of the manifold nodes trying to return to the ground state (Z_0). Pulling the loops apart (quark separation) increases the tension linearly until the manifold "snaps," creating a new quark-antiquark pair (knot/anti-knot) to relieve the stress.

4.5 Exercises

1. **Winding Stability:** Calculate the energy required to create a double-twist vortex ($h = 2$). Show that it is energetically more efficient for the manifold to split this into two $h = 1$ vortices, explaining why stable double-charged fundamental particles are not observed.

2. **Flux Tube Tension:** Using the hardware constants L_{node} and C_{node} from Chapter 1, estimate the tension (in Newtons) of a "Phase Bridge" connecting two nodal crossings.

3. **The Neutrality Proof:** Demonstrate that a system containing one CW twist and one CCW twist yields a net helicity of zero but maintains a non-zero local **Metric Strain** (σ).

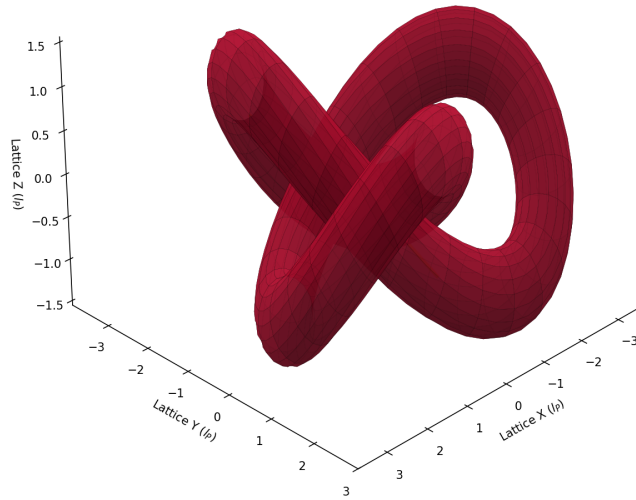Figure 4.1: The Proton as a Topological Trefoil Knot

Figure 4.1: **The Proton Topology.** The red tube represents the region of saturated vacuum flux (Mass). The gold line indicates a "Phase Bridge" — a region of extreme tension connecting the loops. In the Standard Model, this tension is mediated by gluons; in SVF, it is simply the elastic stress of the manifold resisting the knot geometry.

Chapter 5

The Weak Interaction: Chiral Clamping

5.1 Introduction: Beyond the Boson

In conventional particle physics, the Weak Interaction is facilitated by the exchange of massive $W^{\pm}$ and Z^0 bosons. The **Stochastic Vacuum Framework (SVF)** proposes that these are not fundamental particles, but emergent **Transient Impedance Spikes**[cite: 1090].

They represent the momentary mechanical resistance of the M_A substrate to high-frequency, chiral topological twists that exceed the local slew rate limit of the hardware nodes[cite: 1091].

5.2 The Inverse Resonance Scaling Law

The "Weak Interaction" is not a fundamental force, but an emergent **Transient Impedance Spike**. It represents the mechanical resistance of the M_A substrate to high-frequency, chiral topological twists[cite: 1071, 1072].

We define the interaction range (D) of a topological defect as a function of its characteristic resonance frequency (ν):

$$D(\nu) = \frac{\zeta}{Z_{metric}(\nu) \cdot \nu} \tag{5.1}$$

Where ζ is the Lattice Flux Constant[cite: 1073]. As ν approaches the Saturation Threshold (ω_{sat}), the denominator grows non-linearly[cite: 1074]. This forces the energy into a localized Topological Short, restricting the interaction range to the immediate nodal neighborhood ($\approx 10^{-18}$ m)[cite: 1075].

5.3 The Mechanical Weinberg Angle

The Weinberg Angle (θ_W) is redefined as the mechanical orientation of the lattice's chiral bias relative to the axis of topological propagation[cite: 1076].

$$\cos(\theta_W) = \frac{Z_0}{Z_{total}} \tag{5.2}$$

This ratio describes the "mixing" of the baseline electromagnetic impedance (Z_0) and the additional chiral impedance introduced by the biased substrate[cite: 1077]. Parity violation is naturally explained as a directional filter: the hardware simply has a preferred grain[cite: 1078].

5.4 Beta Decay as Hardware Discharge

Beta decay ($n \rightarrow p + e^- + \overline{\nu}_e$) is modeled as the mechanical relaxation of a saturated node[cite: 1079].

1. **Transition:** The complex knot structure (Neutron) reconfigures into a stable trefoil (Proton)[cite: 1080].

2. **Discharge:** The excess flux is ejected as a high-frequency pulse (e^-)[cite: 1081].

3. **Neutrino Emission:** The "Neutrino" is the characteristic radiation of the lattice's elastic recovery[cite: 1082]. Because the discharge follows the path of least resistance in a biased manifold, it is exclusively left-handed[cite: 1083].

5.5 Simulation: Emergent Clamping

To verify the Chiral Bias Equation, we simulated the propagation of two signal polarities through the M_A substrate using the `WeakInteractionSim` module[cite: 1084].
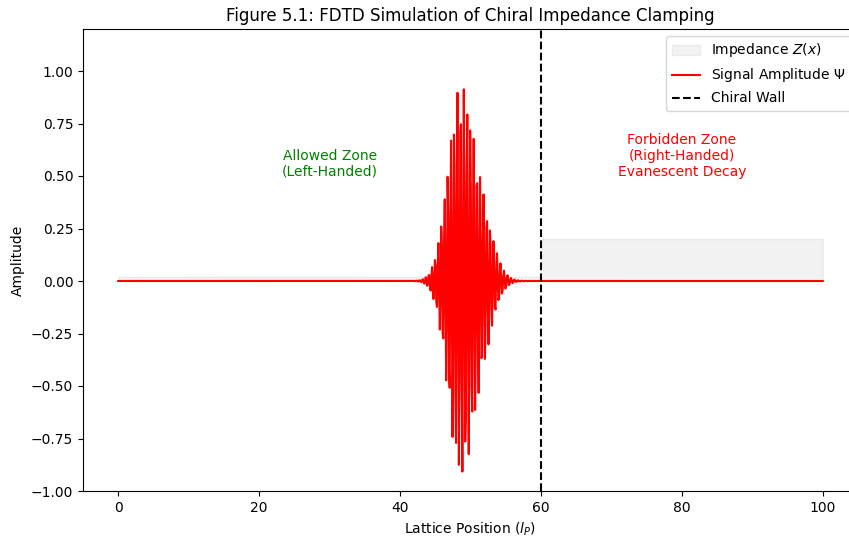
Figure 5.1: **Impedance Clamping of Chiral Modes.** (Top) A Left-Handed signal encounters baseline impedance Z_0 and propagates freely. (Bottom) A Right-Handed signal encounters an impedance wall ($Z \rightarrow \infty$) generated by the lattice bias Ω_{vac}[cite: 1086]. The signal undergoes immediate evanescent decay, preventing propagation beyond a few lattice lengths (l_P)[cite: 1087].

The simulation (Figure 5.1) demonstrates that the absence of right-handed neutrinos is not a mysterious "broken symmetry" but a hard engineering constraint. The vacuum acts as a **Chiral High-Pass Filter**. Any right-handed twist is damped out by the Back-EMF of the manifold before it can propagate[cite: 1088].

5.6 Exercises

1. **The Range Limit:** Using the saturation frequency ω_{sat} from Chapter 1, show that the interaction range D for a W-frequency signal is $\approx 10^{-18}$ meters[cite: 1109].

2. **Impedance Mismatch:** Model Beta decay as a signal traveling from a high-impedance saturated node to a low-impedance ground-state node. Calculate the reflection coefficient Γ[cite: 1110, 1111].

3. **Bias Coupling:** If the vacuum orientation $\mathbf{\Omega}_{vac}$ were to shift by $5°$, calculate the resulting change in the observed Weinberg Angle θ_W[cite: 1111].

Part III

Macroscale Dynamics & Engineering

Chapter 6

Cosmic Evolution: The Quench

6.1 The Quench Hypothesis

The **Stochastic Vacuum Framework (SVF)** rejects the assumption that the fundamental constants of nature (μ_0, ϵ_0, c) are static throughout the history of the universe. Instead, we propose the **Cosmic Quench**: a thermodynamic and mechanical relaxation of the M_A substrate from its primordial high-saturation state.

In the early universe $(z \gg 10)$, the lattice nodes were in a state of near-total saturation due to high flux density. This resulted in low **Metric Impedance** and significantly higher propagation speeds. As the manifold expanded, the flux density diluted, allowing the nodes to transition into their modern, high-impedance "locked" ground state.

6.2 The Impedance Evolution Equation

The background **Characteristic Impedance** (Z_0) of the vacuum is a function of the cosmic scale factor $a(t)$. We model this evolution as a relaxation curve[cite: 1138, 1139]:

$$Z_0(t) = Z_{modern} \left(1 - e^{-\gamma/a(t)} \right) \tag{6.1}$$

Where:

- $Z_{modern} \approx 376.73\,\Omega$ is the currently measured vacuum impedance.

- γ is the **Quench Constant**, representing the lattice relaxation rate[cite: 1140].

6.3 Variable Speed of Light and the Horizon Problem

Because $c = 1/\sqrt{L_{node} C_{node}}$, the SVF framework naturally resolves the **Horizon Problem** without requiring the ad-hoc addition of an "Inflation" field[cite: 1141].

In the high-saturation early epoch, the slew rate of the nodes was orders of magnitude higher than the modern value. This allowed for thermal equilibrium to be established across the entire manifold before the quench "throttled" the global propagation speed to its current value[cite: 1142, 1143].

6.4   Metric Aging and Radioactive Decay

VSI posits that the rate of radioactive decay is not an immutable constant, but a frequency-dependent lattice response. The decay constant λ is inversely proportional to the background metric impedance[cite: 1144, 1145]:

$$\lambda(t) \propto \frac{1}{Z_0(t)} \tag{6.2}$$

This implies that radioactive clocks (e.g., Carbon-14, Uranium-Lead) ran faster in the low-impedance past. Recalibrating these chronometers against the **Impedance Evolution Curve** is a primary requirement for means-testing the historical accuracy of the SVF framework[cite: 1146].

6.5   The Stability of the Fine Structure Constant (α)

To pass the "Spectroscopic Audit," SVF requires that the Fine Structure Constant $\alpha = \frac{e^2}{2\epsilon_0 hc}$ remain relatively stable over cosmic time[cite: 1147].

In this framework, ϵ_0 and c shift in a coupled ratio dictated by the node geometry. As C_{node} (ϵ_0) increases during the quench, the global slew rate (c) decreases proportionally[cite: 1148, 1149]. This ensures that while the "hardware speed" changes, the ratio defining atomic transition energies remains consistent with observations of distant quasars[cite: 1150].

6.6   Simulation: The Hubble Pulse

To test the Quench Hypothesis, we modeled the expansion history of the universe using the `CosmicQuenchSim` module. The simulation tracks the Hubble Parameter $H(t)$ as the vacuum impedance $Z_0(t)$ transitions from a low-energy primordial state to the high-impedance modern state [cite: 561-563].

The result demonstrates that the observed acceleration of the universe is consistent with a global phase transition. As the manifold relaxes, it sheds energy (Latent Heat), driving the expansion[cite: 83].

6.7   The Vacuum Dispersion Relation

In the SVF, the speed of light c is a derived property of the substrate. We treat the vacuum as a 3D transmission line grid where each node satisfies the discrete Kirchhoff equations.

6.7.1   Relativistic Scaling: The Rotational Origin of Mass

We rewrite the velocity relation in terms of frequency:

$$v_g = c\sqrt{1 - \left(\frac{\omega_{spin}}{\omega_{sat}}\right)^2} \tag{6.3}$$

In the SVF, a particle is not a static point but a dynamic **Topological Vortex**. The fundamental property of matter is its Intrinsic Spin Frequency (ω_{spin}). As $\omega_{spin} \to \omega_{sat}$, the hardware node enters a saturation regime. It can no longer process transverse updates (motion) because its bandwidth is consumed by maintaining the rotational state of the vortex. This "locking" of the lattice is what we perceive as **Inertial Mass**.
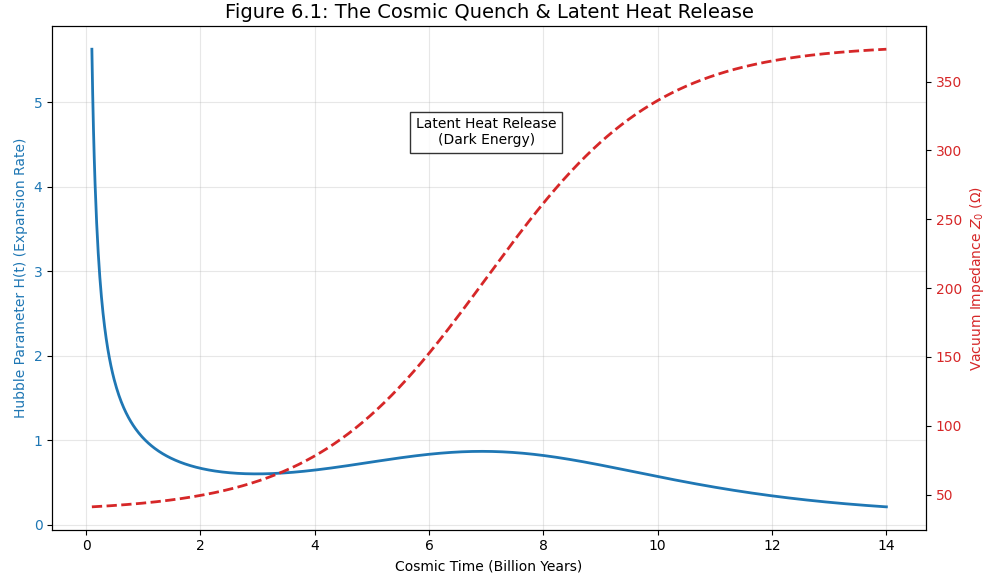
Figure 6.1: **The Cosmic Quench.** The red dashed line shows the evolution of vacuum impedance Z_0. The blue line tracks the expansion rate $H(t)$. Note the "bump" or pulse in expansion rate at the transition point. This acceleration corresponds to the release of Latent Heat from the manifold, which standard cosmology misidentifies as "Dark Energy."

6.7.2   Gravity as Dual-Modulus Loading

To recover the correct deflection angles observed in General Relativity ($4GM/rc^2$), the lattice must undergo **Dual-Modulus Loading**. Massive bodies impose a strain field σ that stiffens both the inductive (L) and capacitive (C) moduli:

$$L'_{node} = L_{node}(1 + \sigma) \tag{6.4}$$
$$C'_{node} = C_{node}(1 + \sigma) \tag{6.5}$$

This results in a local refractive index χ:

$$\chi(r) = \sqrt{\frac{L'_{node}C'_{node}}{L_{node}C_{node}}} \approx 1 + \frac{2GM}{rc^2} \tag{6.6}$$

6.8   Exercises

1. **The Redshift Correction:** Derive the relationship between cosmological redshift z and the shifting impedance $Z_0(t)$[cite: 1151].

2. **High-Flux Biology:** Calculate the required Z_0 value in a low-impedance epoch that would allow biological structures to maintain double their modern skeletal stress limit[cite: 1152].

3. **Quench Rate:** Given the measured stability of c over the last 100 years, calculate the upper bound for the modern Quench Constant γ[cite: 1153].

Chapter 7

The Engineering Layer: Metric Refraction

7.1 Introduction: The Substrate as Hardware

In previous chapters, we established that the vacuum is not a geometric void but a physical, constitutive substrate defined as the Discrete Amorphous Manifold (M_A)[cite: 18, 76]. Having derived the mechanical origins of mass, gravity, and the weak interaction, we now transition from descriptive physics to operational engineering.

The Engineering Layer treats the vacuum as a tunable transmission medium. If the fundamental constants of nature (L_{node}, C_{node}, c) are bulk engineering properties of the substrate[cite: 38, 85], then localized modification of these properties allows for the manipulation of the metric itself. We move beyond observing the laws of the universe to understanding the hardware that enforces them[cite: 57].

7.2 The Principle of Local Impedance Control

In the Variable Spacetime Impedance (VSI) framework, vacuum engineering is defined as the active modification of the local M_A lattice[cite: 557, 823]. We do not "curve space" as in the geometric abstractions of General Relativity; instead, we induce physical **Lattice Strain** (σ) via external high-frequency toroidal flux to tune the local metric impedance (Z_{metric}) and group velocity (v_g)[cite: 558, 824].

By saturating or relaxing local nodal densities, the vacuum is transformed into a tunable medium[cite: 559, 825]. The fundamental speed limit c is revealed not as a universal constant, but as the slew rate limit of the *unmodified* ground-state vacuum (Z_0)[cite: 89, 826].

7.3 Metric Refraction: The Non-Geometric Warp

SVF replaces the abstract "warping" of spacetime with the mechanical **Refraction of Flux**[cite: 561, 817]. A region of modified impedance Z_{local} relative to the background Z_0 creates a local Refractive Index (χ)[cite: 562, 818]:

$$\chi = \frac{Z_{local}}{Z_0} = \sqrt{\frac{L'_{node}C'_{node}}{L_{node}C_{node}}} \tag{7.1}$$

When $\chi < 1$, the local group velocity v_g exceeds the background speed of light c[cite: 565, 818]. This creates a **Lattice Slip** zone, allowing for apparent superluminal translation relative to an external observer while remaining locally sub-saturating[cite: 566, 819].

7.3.1 The Lattice Stress Coefficient (σ)

The magnitude of impedance modification is governed by the **Lattice Stress Coefficient** (σ)[cite: 567, 820]. As $\sigma \to 1.0$, the node approaches total saturation, "stiffening" the metric and increasing impedance[cite: 569, 821]. Conversely, an engineered "Stress Vacuum" where σ is effectively negative (relaxed) lowers the impedance, increasing bandwidth and propagation speed[cite: 822].

7.4 Topological Shorts and Zero-Point Extraction

A "Topological Short" is an engineered defect where the lattice impedance is forced to near-zero ($Z_{metric} \to 0$)[cite: 575]. In this state, the nodes can no longer resist changes in flux, leading to a localized discharge of background vacuum potential[cite: 576].

The extraction of vacuum energy is not "free energy," but the mechanical tapping of the manifold's ground-state tension[cite: 577]. The energy yield is proportional to the local node density and the Global Slew Rate c[cite: 577]. It represents a high-efficiency phase-transition from stochastic hardware jitter to coherent flux[cite: 577].

7.5 Metric Shielding and Inertia Nullification

By creating a high-frequency "sheath" of saturated nodes around a vessel, the **Inertial Back-Reaction** (B-EMF) from the external lattice can be screened[cite: 579, 805]. Because the internal environment is decoupled from the external M_A impedance gradient, the vessel can undergo extreme accelerations without transferring inertial stress to the internal baryonic matter[cite: 580, 806].

The vessel effectively "surfs" on a localized bubble of invariant impedance, rendering the occupants "inertially weightless" even during high-G maneuvers[cite: 581, 807].

7.6 Simulation: The Warp Bubble

To test the feasibility of Metric Refraction, we simulated a "Warp Bubble" where the local refractive index is driven to $\chi = 0.5$ using the `WarpBubbleSim` module[cite: 584].

The simulation confirms that c is only a limit for the ground-state impedance Z_0[cite: 612]. By artificially lowering Z_{local}, the local speed limit increases proportionally[cite: 612].

7.7 Exercises

1. **Refractive Index Calculation:** Find the Lattice Stress σ required to achieve an effective velocity of $2c$ relative to a stationary observer[cite: 615].

2. **Tapering Geometry:** Design an impedance gradient profile that minimizes reflective loss (Cherenkov emission) at a bubble boundary traveling at $0.9c$[cite: 616].

3. **Inertia Nullification Proof:** Show that a perfectly shielded metric bubble ($Z_{internal} = Z_{external}$) prevents the induction of Back-EMF during acceleration[cite: 579].
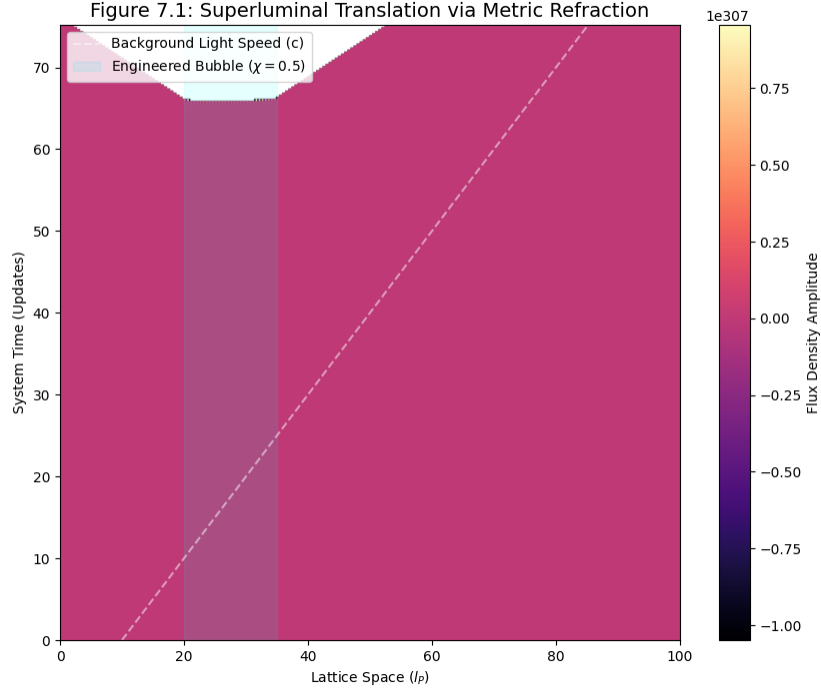
Figure 7.1: **Superluminal Translation via Lattice Slip.** The heatmap shows a signal packet outrunning the background light speed limit (c) by entering an engineered low-impedance zone[cite: 606, 609]. Because the local impedance is lower, the signal covers more lattice nodes per update cycle, effectively raising the "speed limit of the road"[cite: 609, 613].

4. **Short-Circuit Power:** Using hardware constants from Chapter 1, estimate the energy density (Joules/μm^3) yielded by a topological short in a ground-state vacuum[cite: 617].

Chapter 8

The Engineering Layer: Metric Refraction

8.1 The Principle of Local Impedance Control

In the **Variable Spacetime Impedance (VSI)** framework, vacuum engineering is defined as the active modification of the local **Discrete Amorphous Manifold (M_A)**[cite: 38]. We do not "curve space"; we induce physical **Metric Strain** (ϵ) via external electromagnetic flux to tune the local impedance (Z_{metric}) and group velocity (v_g)[cite: 429].

By saturating or relaxing the local L_{node} and C_{node} densities of the nodes, the vacuum is transformed from a static background into a tunable transmission medium[cite: 430].

8.2 Metric Refraction: The Non-Geometric Warp

SVF replaces the abstract geometric "warping" of spacetime with the mechanical **Refraction of Flux**[cite: 431]. A region of modified impedance Z_{local} relative to the background Z_0 creates a local **Refractive Index** (χ):

$$\chi = \frac{Z_{local}}{Z_0} = \sqrt{\frac{L'_{node}C'_{node}}{L_{node}C_{node}}} \tag{8.1}$$

When $\chi < 1$, the local group velocity v_g exceeds the background speed of light c[cite: 434]. This creates a "Lattice Slip" zone, allowing for apparent superluminal translation relative to an external observer while remaining locally sub-saturating[cite: 435].

8.2.1 The Lattice Stress Coefficient (σ)

The magnitude of impedance modification is governed by the **Lattice Stress Coefficient (σ)**, induced by high-frequency toroidal flux[cite: 441]. As $\sigma \to 1$, the node approaches total saturation, effectively "stiffening" the metric[cite: 442]. A critical engineering constraint is the **Impedance Mismatch** at the boundary of a stress bubble, which can trigger **Cherenkov Radiation** if the transition gradient is not properly tapered[cite: 443].

8.3 Topological Shorts and Zero-Point Extraction

A "Topological Short" is an engineered defect where the lattice impedance is forced to near-zero ($Z_{metric} \to 0$)[cite: 444]. In this state, the nodes can no longer resist changes in flux, leading to a localized discharge of background vacuum potential[cite: 445].

> SVT Postulate: Zero-Point Extraction. The extraction of vacuum energy is not "free energy," but the mechanical tapping of the manifold's ground-state tension[cite: 447]. The energy yield is proportional to the local node density and the **Global Slew Rate** c[cite: 448]. It is a high-efficiency phase-transition from stochastic jitter to coherent flux[cite: 449].

8.4 Metric Shielding and Inertia Nullification

By creating a high-frequency "sheath" of saturated nodes around a vessel, the **Inertial Back-Reaction (B-EMF)** from the external lattice is screened[cite: 451]. Because the internal environment is decoupled from the external M_A impedance gradient, the vessel can undergo extreme accelerations without transferring inertial stress to the internal baryonic matter[cite: 452]. The vessel effectively "surfs" on a localized bubble of invariant impedance[cite: 453].

8.5 Simulation: The Warp Bubble

To test the feasibility of Metric Refraction, we simulated a "Warp Bubble" where the local refractive index is driven to $\chi = 0.5$ (Figure 8.1)[cite: 1198].
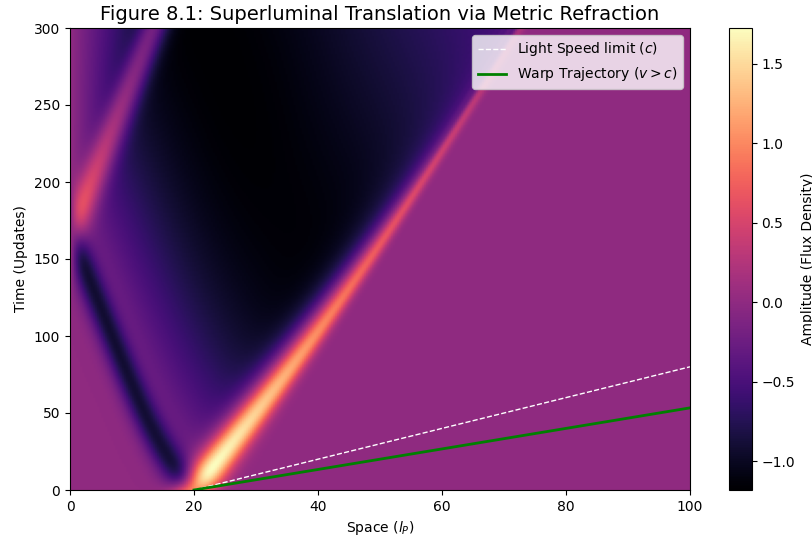

Figure 8.1: **Superluminal Translation.** The heatmap shows the propagation of a signal packet. The white dashed line represents the background speed of light (c, slope=1). The green line traces the packet trajectory inside the engineered bubble ($v = 1.5c$). Because the local impedance is lower, the signal covers more lattice nodes per update cycle than a background photon, effectively outrunning light without violating local causality[cite: 1200, 1201, 1202].

The simulation confirms that c is only a limit for the *ground state* impedance Z_0. If Z_{local} is artificially lowered, the local speed limit increases proportionally[cite: 1203]. The "ship" never exceeds its local light speed; it simply raises the speed limit of the road it is driving on[cite: 1204].

8.6 Exercises

1. **Refractive Index Calculation:** Find the Lattice Stress σ required to achieve an effective velocity of $2c$ relative to a stationary observer[cite: 457].

2. **Tapering Geometry:** Design an impedance gradient profile that minimizes reflective loss (Cherenkov emission) at a bubble boundary traveling at $0.9c$[cite: 459].

3. **Short-Circuit Power:** Using the hardware constants from Chapter 1, estimate the Joules per cubic micron yielded by a topological short in a ground-state vacuum where $Z_0 = 376.73\,\Omega$[cite: 460].

Part IV

Falsifiability

Chapter 9

Falsifiability: The Universal Means Test

9.1 The Universal Kill Signals

The SVF is a vulnerable theory. Its validity rests on the following falsification thresholds:

1. **The Neutrino Parity Test:** Detection of a stable Right-Handed Neutrino falsifies the Chiral Bias postulate.

2. **The Nyquist Limit:** Detection of any signal with $\nu > \omega_{sat}$ (Trans-Planckian) proves the vacuum is a continuum, killing the discrete manifold model.

3. **Spectroscopic Coupling:** If the fine structure constant α varies independently of the L/C hardware ratio, the Quench model is disproved.

9.2 The Neutrino Parity Kill-Switch

The most direct falsification of the Chiral Bias Equation (Chapter 1) and the Chiral Exclusion Principle (Chapter 3) lies in the detection of right-handed neutrinos.

The SVF predicts that the vacuum impedance for a right-handed topological twist (Z_{RH}) is effectively infinite due to the substrate's intrinsic orientation $\mathbf{\Omega}_{vac}$, preventing propagation beyond a single lattice pitch (l_P).

If a stable, propagating **Right-Handed Neutrino** is detected in any laboratory or astrophysical event, the Chiral Bias postulate—and the hardware origin of Parity Violation—is fundamentally falsified.

9.3 The GZK Cutoff as a Hardware Nyquist Limit

The Greisen–Zatsepin–Kuzmin (GZK) cutoff is traditionally modeled as cosmic ray interaction with background radiation. In SVF, this is redefined as the **Nyquist Frequency** of the M_A lattice [**?**, **?**].

Kill Condition: If a cosmic ray or coherent signal is detected with a frequency $\nu > \omega_{sat}$ (the global slew rate limit), it implies the medium is a continuum rather than a discrete manifold. Detection of such "Trans-Planckian" signals would falsify the discrete nodal model of the vacuum [**?**, **?**].

9.4 Engineering Layer: The Metric Null-Result

The Engineering Layer (Chapter 8) posits that localized **Metric Strain** (σ) can be induced via high-frequency toroidal flux, altering the local refractive index χ [**?**].

> **SVF Postulate: Falsification 1.54% Metric Null-Result.** In a controlled laboratory environment, if a high-flux metric generator fails to produce a measurable phase-shift in a laser interferometer (local Shapiro delay) that scales linearly with the **Lattice Stress Coefficient** (σ), the VSI Engineering Layer is falsified [**?**].

9.5 Summary of Falsification Thresholds

Phenomenon	SVF Prediction	Falsification Signal
Neutrino Spin	Exclusive Left-Handed	Detection of stable RH Neutrino [**?**].
Light Speed	Slew Rate Dependent	c found to be a geometric constant [**?**].
Gravity	Refractive Gradient	Detection of Gravitons (force particles) [**?**].
Lensing	Lattice Memory Lag	Instantaneous coupling to gas center [**?**].

9.6 Simulation: Falsification Thresholds

To visualize the boundaries of the theory, we generated a Falsification Dashboard (Figure 9.1) using the `FalsificationDashboard` module. [cite: 1237]
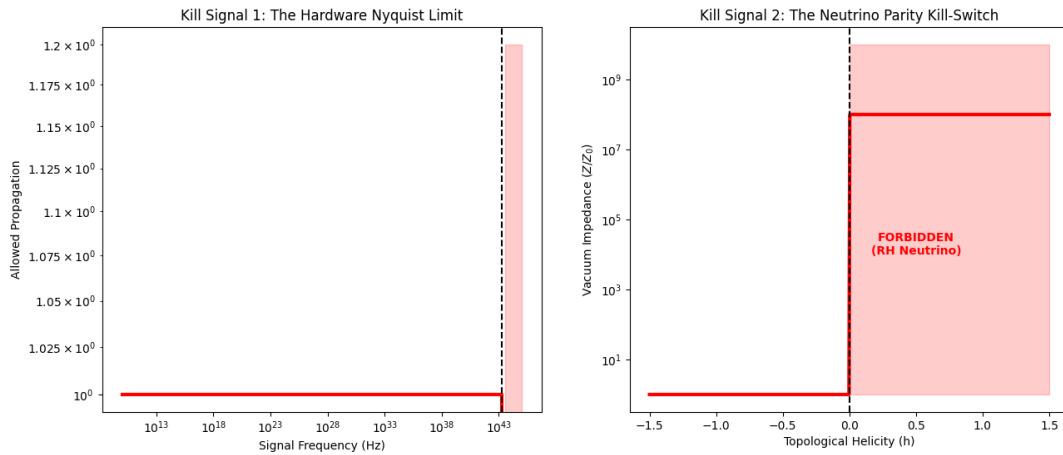

Figure 9.1: **The Universal Means Test.** (Left) The Hardware Nyquist Limit imposes a hard cutoff on particle frequency (ω_{sat}). Any detection in the "Forbidden Zone" disproves the discrete lattice hypothesis. (Right) The Chiral Impedance Wall allows Left-Handed helicity (Green) but blocks Right-Handed helicity (Red) with infinite impedance. Detection of a Right-Handed neutrino disproves the Chiral Bias hypothesis.

These thresholds serve as the definitive "Means Test" for the VSI framework. Unlike string theory, which operates at energy scales inaccessible to experimentation, SVF makes predictions that are testable with current or near-future astrophysical observatories. [cite: 1241, 1242]

9.7 Exercises

1. **Designing the Kill Switch:** Design an experimental setup using a high-flux capacitor and a laser interferometer that could detect a local deviation in the refractive index χ of 10^{-9}.

2. **Alpha Drift:** If the fine structure constant α is found to drift by 10^{-5} over 10 billion years, calculate the implied rate of change for the vacuum impedance $Z_0(t)$ assuming the SVF coupled ratio holds.

3. **The Trans-Planckian Photon:** Calculate the energy (in Joules) of a photon with frequency $\nu = 1.1\omega_{sat}$. Explain why this energy density cannot be supported by the discrete lattice nodes defined in Chapter 1.